IFAR Liner Benchmark Challenge #1 - DLR Impedance Eduction of Uniform and Axially Segmented Liners and Comparison with NASA Results

Friedrich Bake[1], Ralf Burgmayer[1], Anita Schulz[1], Karsten Knobloch[1], Lars Enghardt[1], and Michael G. Jones[2]

Abstract

This paper presents the contribution from the German Aerospace Center (DLR) to the first liner benchmark challenge under the framework of the International Forum for Aviation Research (IFAR). Therefore, two sets of acoustically damping wall treatments, called 'liner samples', have been produced by additive manufacturing based on the design data provided by NASA coordinating this benchmark. These liner samples have been integrated and acoustically characterized in the liner flow test facility DUCT-R at DLR Berlin as well as in the liner flow test facility GFIT at NASA Langley. Besides the dissipation coefficients and the axial pressure profiles, the liner wall impedance was educed by first determining the axial wave numbers and then applying a straightforward method based on the one-dimensional Convected Helmholtz Equation. Finally, the comparison of the liner impedance values to the NASA results show a fairly good agreement.

Keywords

Liner characterization, Impedance eduction, Liner test facilities, IFAR benchmark

[1]German Aerospace Center (DLR), Germany
[2]NASA Langley Research Center, USA

Corresponding author:
Friedrich Bake, German Aerospace Center (DLR),
Institute of Propulsion Technology, Department of Engine Acoustics, Mueller-Breslau-Str. 8, 10623 Berlin, Germany.
Email: friedrich.bake@dlr.de

Introduction

Liners as a wall treatment for acoustic damping are one of the most important technologies for aircraft noise reduction. They are usually integrated in the inlet and bypass duct of aero-engines in order to reduce the engine noise emission propagating from various internal sources. Although there exist fairly mature technology solutions for liner design, the predictive capabilities of liner performance under real application conditions are still unsatisfactory. There remains the need for experimental testing of liner samples in purpose-built liner flow duct facilities. This yields the challenge to ensure comparability between the different liner test facilities existing worldwide and the correspondingly applied post-processing methods and prediction approaches.

To address this challenge, the International Forum for Aviation Research (IFAR) initiated a benchmark activity devoted to compare acoustic liner testing and performance prediction. The DLR Department of Engine Acoustics took part in this liner benchmark managed by NASA. The liner benchmark is divided into three different challenges:

- Challenge #1: Comparison of Liner Test Facilities
- Challenge #2: Propagation Code Comparison
- Challenge #3: Impedance Eduction Comparison

This paper will mainly focus on the DLR contribution to Challenge #1 and a corresponding comparison to NASA results. For Challenge #1, NASA provided CAD drawings of selected generic liner designs to all participating partners within IFAR. Two liner configurations are considered for this challenge. The first is a uniform liner, for which the impedance should be nearly constant over the length of the liner. The second is a two-segment liner, where the only difference between the two axial segments is the depth of the liner cavity. Measurement results from these liner configurations have been published by NASA in Jones et al. [1,2].

The goal of Challenge #1 is to gather data from multiple test rigs with the same liner configurations manufactured using 3D printing. By sharing the data with each participant, it will be possible to evaluate dependence of these results on fabrication, data acquisition and analysis (e.g., impedance eduction) approaches. Within this paper the DLR contribution to Challenge #1 and the comparison of the DLR results with NASA data will be presented.

IFAR Challenge #1 liner geometries

The two liner configurations of IFAR Challenge #1 are shown in Figure 1. The first, homogeneous liner sample **IFAR1** (Figure 1, left) has a constant cavity depth of 50.8 mm (corresponds to $2.0''$, called D2) and the second liner sample **IFAR2** (Figure 1, right) has one part with a cavity depth of 50.8 mm ($2.0''$) and another part with a cavity depth of 76.2 mm ($3.0''$, called D3). Both liner samples consist of 4-by-30 liner cavities. The liner cavity dimensions are 10.2 mm ($0.4''$) by 10.2 mm ($0.4''$) with an axial partition thickness of 3.4 mm and a spanwise partition thickness of 3.3 mm giving a total length of 406.4 mm ($16''$) and a total width of 57.5 mm. Each liner cavity has 22 holes with a nominal diameter of 1.1 mm as shown in Figure 2, yielding a porosity of about 12%, including partition thicknesses. The face sheet has a thickness of 0.8 mm.

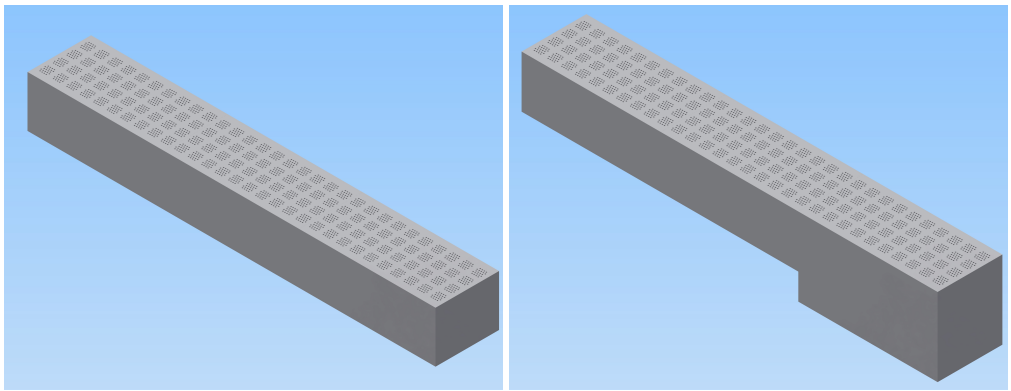

Figure 1. CAD models of the liner samples (left: constant depth liner **IFAR1**; right: two-segment liner **IFAR2**).

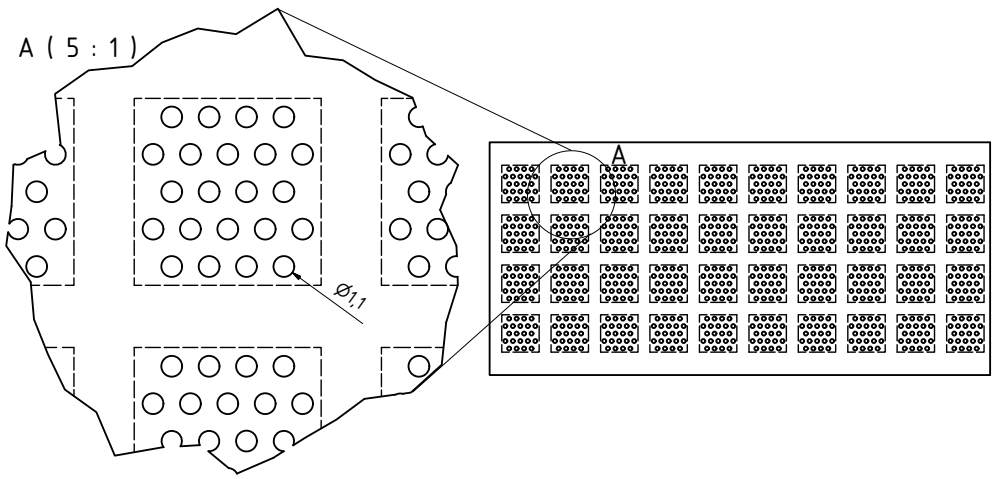

Figure 2. Detailed sketch of the liner facesheet geometry.

NASA GFIT facility and NASA impedance eduction method

The NASA Langley Grazing Flow Impedance Tube (GFIT, see Figure 3) has a 50.8 mm-wide ($2.0''$) by 63.5 mm-high ($2.5''$) cross-sectional geometry, and allows evaluation of acoustic liners with lengths from 50.8 mm to 609.6 mm. The surface of the test liner (highlighted in blue) forms a portion of the upper wall of the flow duct. Twelve acoustic drivers form an upstream (exhaust mode) source and six acoustic drivers form a downstream (inlet mode) source. The results in this study were attained using the upstream source. There are 53 microphones flush-mounted in the lower wall (opposite the liner) of the GFIT. The data presented in this study were acquired using a stepped-sine source (one frequency at a time) over a

frequency range of 0.4 to 3.0 kHz, at a source SPL (peak total SPL measured near the liner leading edge) of 140 dB and centerline Mach numbers of 0.0 and 0.3.

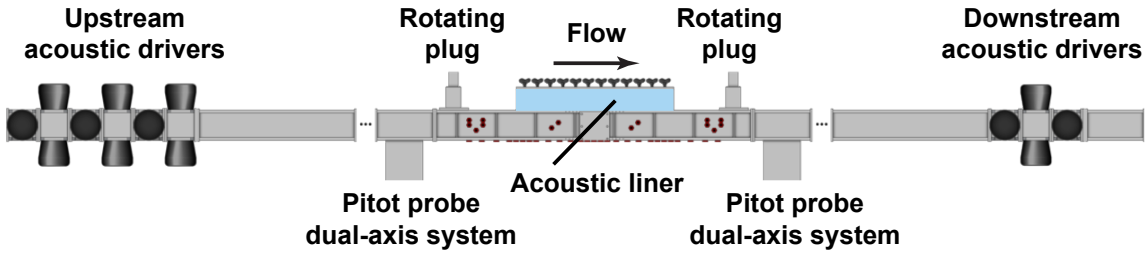

Figure 3. Sketch of the NASA Grazing Flow Impedance Tube (GFIT). Microphones depicted as small cylinders, placed on all walls surrounding the acoustic liner section.

The impedance of the constant depth liner (**IFAR1**) was educed using a Kumaresan and Tufts (KT) method, which is explained in detail by Jones et al.[1]. This method is very similar to the impedance eduction technique applied by DLR and described in the next sections.

For the two-segment liner (**IFAR2**), an indirect method based on a finite element solution to the convected Helmholtz equation (CHE) is used to educe the liner impedance. This method assumes the flow is uniform and the sound fields upstream ($0 \leq x \leq x_1$) and downstream ($x_2 \leq x \leq L$) of the liner (see Figure 4) contain no higher-order modes. Under these assumptions, the acoustic field satisfies a convected Helmholtz equation on the acoustic pressure fields (assuming an $e^{i\omega t}$ time dependence)

$$\left(1-M^2\right)\frac{\partial^2 p(x,y)}{\partial x^2}+\frac{\partial^2 p(x,y)}{\partial y^2}-2ikM\frac{\partial p(x,y)}{\partial x}+k^2 p(x,y)=0. \tag{1}$$

The local-reacting wall boundary condition presented by Myers[3] is given by

$$-\frac{\partial p(x,H)}{\partial y}=ik\left(\frac{p(x,H)}{\zeta}\right)+2M\frac{\partial}{\partial x}\left(\frac{p(x,H)}{\zeta}\right)+\frac{M^2}{ik}\frac{\partial^2}{\partial x^2}\left(\frac{p(x,H)}{\zeta}\right), \tag{2}$$

where the normalized admittance, $1/\zeta$, is taken as zero along the rigid wall portion of the upper wall and H is the duct height (63.5 mm (2.5″) for the GFIT). The normal component of the acoustic particle velocity vanishes at the rigid lower wall

$$\frac{\partial p(x,0)}{\partial y}=0, \tag{3}$$

and the source and exit plane acoustic pressures are assumed known from measurements on the lower wall

$$p(0,y)=p(0,0);\;\; p(L,y)=p(L,0). \tag{4}$$

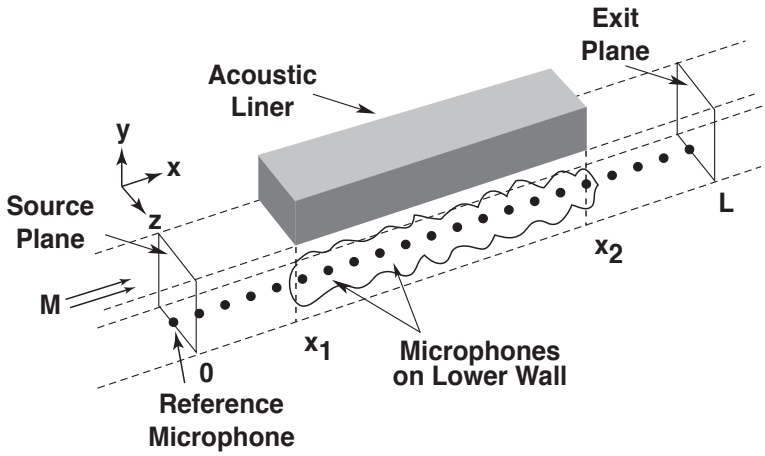

Figure 4. Sketch of computational domain in GFIT.

If the acoustic impedance of the liner is known, Equations (1) - (4) may be solved via a finite element method to determine the acoustic pressure field throughout the GFIT. Instead, the CHE method employs an optimizer to search for an impedance where the acoustic pressures predicted via this finite element method match the corresponding acoustic pressures measured with the microphones along the lower wall of the GFIT to within an acceptable tolerance. This impedance is taken to be the impedance of the liner.

DLR DUCT test rig and liner manufacturing

The DLR liner test facility DUCT-R consists of a flow duct with a cross-section of 60 mm (W) by 80 mm (H). Driven by an upstream radial compressor a mean flow Mach number on the centerline of up to 0.3 can be set. The duct itself is setup symmetrically with loudspeakers (A and B) at the upstream and downstream ends, two (hard-wall) measurement sections and a liner mounting module (face-to-face section) in the center as shown in the schematic sketch in Figure 5.

Microphones are installed at different axial positions in both the hard wall measurement sections as well as face-to-face in the liner module. The face-to-face microphones are flush-mounted in the wall on the opposite side of the liner surface. Figure 6 shows a photo of the DUCT-R setup applied for this investigation. Further details about the test rig and the acoustic measurements system can also be found in Busse-Gerstengarbe et al.[4] and in Schulz et al.[5]. The variety of microphone positions enables the evaluation of the scattering coefficients (reflection, transmission and dissipation) of the liner module via the hard-wall measurement sections and the acquisition of the sound field directly in the lined duct section via the face-to-face microphones. From both data sets, determination of the liner impedance is possible using various eduction methods. This includes modal and nonmodal based impedance eduction approaches as described in Weng et al.[6]. The acoustic excitation was accomplished using single tones with an incident sound wave amplitude of approximately 140 dB.

The provided CAD was modified to increase the thickness of the outer axial partitions to 6.3 mm in order to fit into the liner mounting device of the DLR liner test facility DUCT-R. However, this

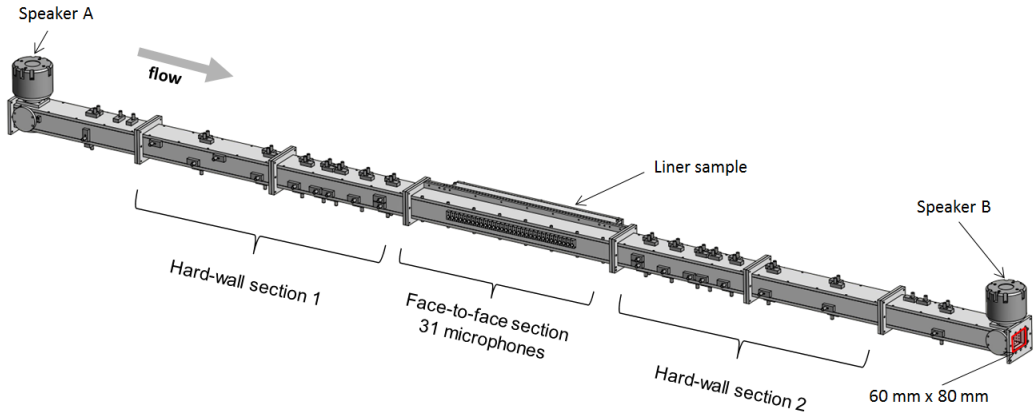

Figure 5. Sketch of the DLR liner test facility DUCT-R with the two measurement (hard-wall) sections and the liner mounting module in between.

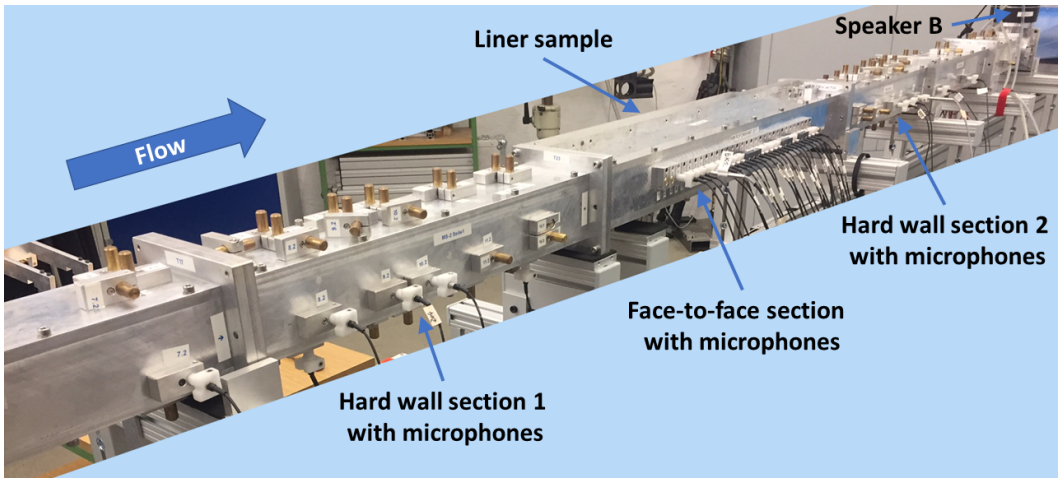

Figure 6. Photo of the DLR liner test facility DUCT-R with the liner mounting module in the center.

adaptation does not change the geometric configuration of the active liner surface as part of the duct wall. The liner samples were fabricated using the 3D-printing stereolithography process with indurating liquid photopolymer resin. Since the length of the liner samples exceeds the maximum printable size of our device, the samples were printed in three segments consisting each of 4-by-10 cavities. A 3.8 mm thick aluminum plate was used as a backplate.

A major challenge during manufacturing was to find the best-suited printing configuration for an optimal printing accuracy across the entire spatial range since the size of the liner segments corresponds to almost the maximum permissible printing size of the printer device. For this purpose, a number of

test prints with varying print parameters were conducted. In addition, to further increase manufacturing accuracy, all samples were designed with a 1 mm oversize. During post processing the samples were sanded and the oversize was milled to match the nominal specifications. Subsequently, the segments were evaluated yielding maximum deviations of about 0.05 mm compared to the required specifications. The perforation diameters vary between 1.07 mm and 1.12 mm. The left photo in Figure 7 shows a single liner segment after post processing and the right photo shows the homogeneous liner sample installed in the DUCT-R.

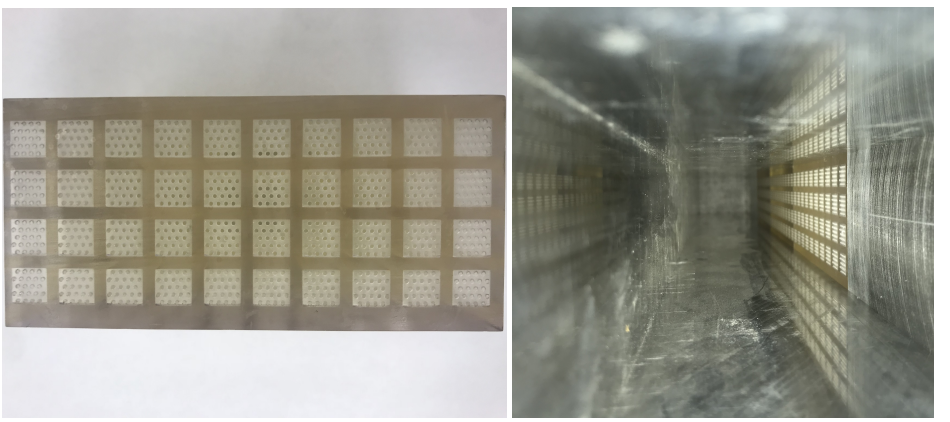

Figure 7. Photos of the 3D printed post processed liners (left: single liner segment; right: liner sample installed in the duct).

DLR data post processing, results and discussion

This section presents the DLR data analysis steps and the corresponding results from the liner samples **IFAR1** and **IFAR2** in comparison to the NASA impedance results.

Scattering coefficients

The damping performance of the liner is evaluated using the dissipation coefficient. This is an integral value of the acoustic power that is absorbed while a sound wave passes the lined element. The determination of the dissipation coefficient is described by Lahiri et al.[7] and based on a method proposed by Ronneberger[8] and his students.[9,10]

For each configuration, two different sound fields are excited consecutively in two separate measurements (indices a and b). Speaker A (upstream) is used in the first measurement and in the second measurement the same signal is fed into speaker B (downstream). Then, the data of section 1 and section 2 (indices 1 and 2) are analyzed separately. This results in four equations for the complex sound pressure amplitudes for each section and measurement:

$$p_{1a}(x) = p_{1a}^{+} e^{-ik_1^{+}x} + p_{1a}^{-} e^{ik_1^{-}x} \tag{5}$$

$$p_{2a}(x) = p_{2a}^{+} e^{-ik_2^{+}x} + p_{2a}^{-} e^{ik_2^{-}x} \tag{6}$$

$$p_{1b}(x) = p_{1b}^{+} e^{-ik_1^{+}x} + p_{1b}^{-} e^{ik_1^{-}x} \tag{7}$$

$$p_{2b}(x) = p_{2b}^{+} e^{-ik_2^{+}x} + p_{2b}^{-} e^{ik_2^{-}x}. \tag{8}$$

p^+ and p^- are the complex amplitudes of the downstream and upstream traveling waves with their respective wave numbers $k^{\pm}$.

According to Equations 5-8 the measured acoustic signal is a superposition of two plane waves traveling in opposite directions. In order to determine the downstream and upstream propagating portions of the wave in each section, Equations 5-8 are fitted to the microphone data. As a result of this least-mean-square fit, the four complex sound pressure amplitudes p_1^+, p_1^-, p_2^+ and p_2^- are identified for both measurements. The respective ratios of these sound pressure amplitudes yield the reflection and transmission coefficients of the test object. This is illustrated in Figure 8 for the two different measurements A and B. The results from both measurements are combined in order to calculate the reflection and transmission coefficients:

$$r^+ = \frac{p_{1a}^- p_{2b}^- - p_{1b}^- p_{2a}^-}{p_{1a}^+ p_{2b}^- - p_{1b}^+ p_{2a}^-} \qquad r^- = \frac{p_{2b}^+ p_{1a}^+ - p_{2a}^+ p_{1b}^+}{p_{1a}^+ p_{2b}^- - p_{1b}^+ p_{2a}^-} \tag{9}$$

$$t^+ = \frac{p_{2a}^+ p_{2b}^- - p_{2b}^+ p_{2a}^-}{p_{1a}^+ p_{2b}^- - p_{1b}^+ p_{2a}^-} \qquad t^- = \frac{p_{1a}^+ p_{1b}^- - p_{1b}^+ p_{1a}^-}{p_{1a}^+ p_{2b}^- - p_{1b}^+ p_{2a}^-}. \tag{10}$$

The advantage of combining the two measurements is that the resulting coefficients are independent from the reflection of sound at the duct terminations. These end-reflections are contained in the equations of the sound pressure amplitudes, but do not need to be calculated explicitly. The analysis is applied only in the plane-wave regime (here up to 2100 Hz) i.e., the acoustic pressure is constant across the duct cross-section. The dissipation coefficient of the acoustic energy can be calculated from the reflection and transmission coefficients via an energy balance:

$$R^{\pm} + T^{\pm} + \Delta^{\pm} = 1. \tag{11}$$

The energy of the incident wave is partly reflected, partly transmitted, and partly absorbed by the damping module. R and T are the power quantities of the reflection and transmission coefficients, while r and t are the corresponding pressure quantities. Blokhintsev[11] defines the acoustic energy flux I in a moving medium (see as well in[12]):

$$I = \frac{1}{\rho c} (1 + M)^2 \left\langle p^2 \right\rangle \tag{12}$$

where $\left\langle p^2 \right\rangle$ is the time-averaged acoustic pressure squared, ρ is the density of the medium, c is the speed of sound, and M is the mean Mach number. Integrating over the duct cross-section area A and using the pressure amplitude yields a relation between the acoustic pressure p and acoustic power P quantities:

$$P^{\pm} = \frac{A}{2\rho c} (1 \pm M)^2 \left| p^{\pm} \right|^2. \tag{13}$$

Applying Equation 13 to R and T in Equation 11 and then solving for Δ with $A_1 = A_2$, $\rho_1 = \rho_2$, $c_1 = c_2$, and $M_1 = M_2 = M$ yields the definition of the energy dissipation coefficient:

$$\Delta^{\pm} = 1 - \left(\frac{(1 \mp M)^2}{(1 \pm M)^2} \cdot \left| r^{\pm} \right|^2 + \left| t^{\pm} \right|^2 \right). \tag{14}$$

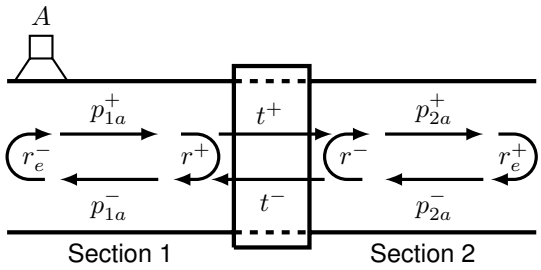

(a) Measurement A, upstream excitation

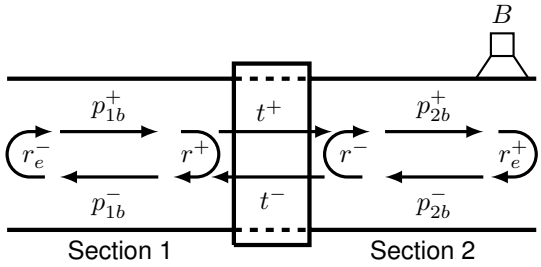

(b) Measurement B, downstream excitation

Figure 8. Illustration of the sound field in the duct for measurements A and B by means of the sound pressure amplitudes p, the reflection coefficient r, the transmission coefficient t, and the end reflection r_e.

This is an integral value of the acoustic energy that is absorbed while a sound wave is passing the damping module.

Figure 9 presents the dissipation coefficient of the **IFAR1** liner sample with the constant cavity depth for the three investigated flow cases:

- no flow
- centerline Mach number: 0.1
- centerline Mach number: 0.3

The left side of Figure 9 shows the dissipation coefficient in the downstream direction, which is in the no flow case (black line) almost identical to the dissipation values in the upstream direction (right side of Figure 9) since the liner sample is symmetric. It provides a resonator liner typical, distinct dissipation maximum here at around 1300 Hz, which broadens with increased grazing flow Mach number. This frequency is presumably related to a quarter-wavelength ($\lambda/4$) resonance in the liner cavity. For a grazing flow Mach number of 0.3, the dissipation maximum for upstream excitation shifts slightly to higher frequencies around 1500 Hz. In the opposite direction against the flow, the broadening of the high dissipation range is stronger as expected. In this case, the transmission coefficient (not shown here) is de facto zero for a frequency range between 1100 Hz and 1400 Hz.

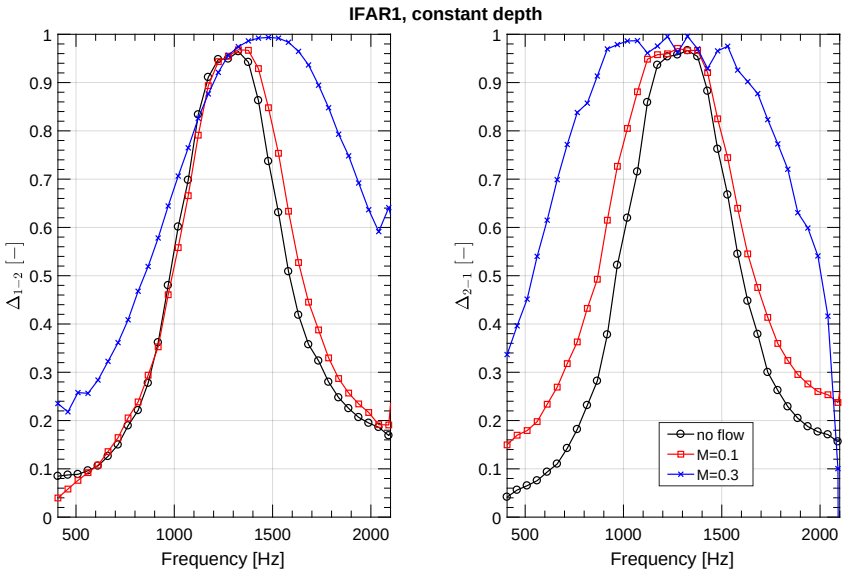

Figure 9. Dissipation coefficient of **IFAR1** liner sample for different flow conditions: no flow (black), centerline Mach number 0.1 (red) and centerline Mach number 0.3 (blue). left: in downstream direction; right: in upstream direction.

The dissipation coefficient of the axially segmented **IFAR2** liner in Figure 10 exhibits for the no flow case (black solid line) two maxima at around 1100 Hz and again at around 1300 Hz. The dissipation coefficient of the **IFAR1** liner sample (black dashed line in Figure 10), which has the same geometrical configuration (D2) as the first segment of **IFAR2** coincides fairly well with the second dissipation maximum. The first dissipation maximum seems to be related to the second axial liner segment with a cavity depth D3. With increasing grazing flow Mach number (red and blue line), a similar broadening effect of the dissipation is observable like for the **IFAR1** liner. At a Mach number of 0.3, the two dissipation maxima almost merge.

Axial pressure profiles

In order to enhance the understanding of the damping characteristics and to prepare the wave number determination in the lined duct sections, Figures 11 (**IFAR1**) and 12 (**IFAR2**) show the axial pressure profile for selected frequencies of the face-to-face mounted microphones in the liner section with the two closest microphones on each side in the hard wall sections. Both figures display the case with upstream excitation (speaker A) and a grazing flow Mach number of $M = 0.3$. The axial position and the length of the lined section is marked with a gray box.

The magnitude of the sound pressure for the **IFAR1** liner sample (constant depth D2) in Figure 11 is strongly decreasing over the lined section for the center frequency of the dissipation maximum (1479 Hz, red line). For the frequency where the dissipation is significantly lower (765 Hz, blue line), the decline in

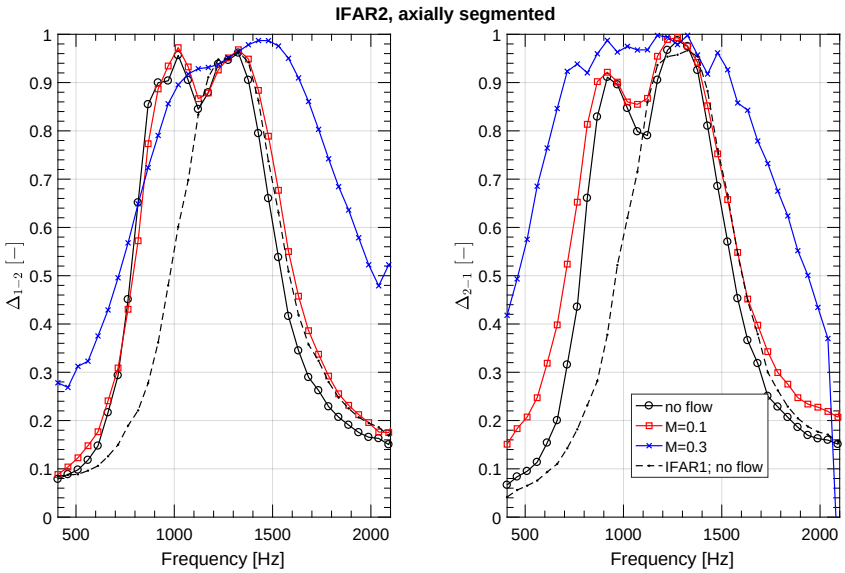

Figure 10. Dissipation coefficient of **IFAR2** liner sample for different flow conditions: no flow (black), centerline Mach number 0.1 (red) and centerline Mach number 0.3 (blue). left: upstream excitation; right: downstream excitation. The black dashed line shows the no flow results of the **IFAR1** sample (constant depth D2).

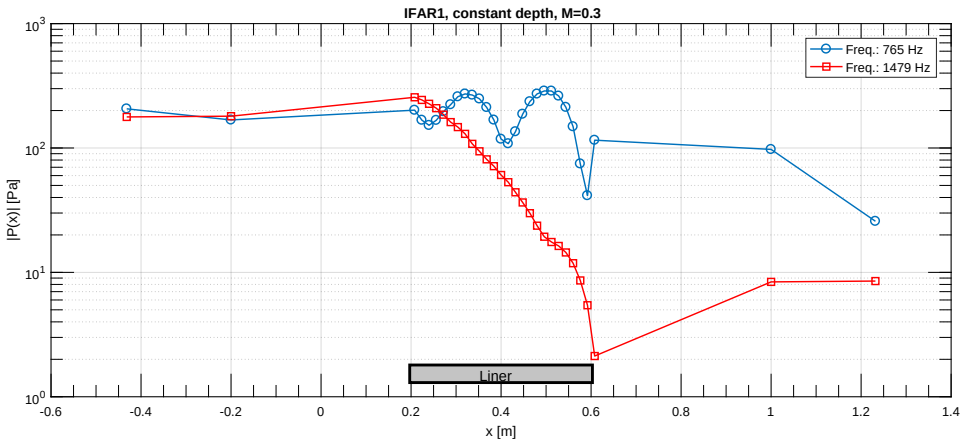

Figure 11. Axial pressure profiles with **IFAR1** liner sample at centerline Mach number 0.3 for two different frequencies: 765 Hz (blue line; low dissipation) and 1479 Hz (red line; high dissipation).

the axial pressure profile is smaller while a standing wave pattern in the lined section due to reflections becomes more prominent.

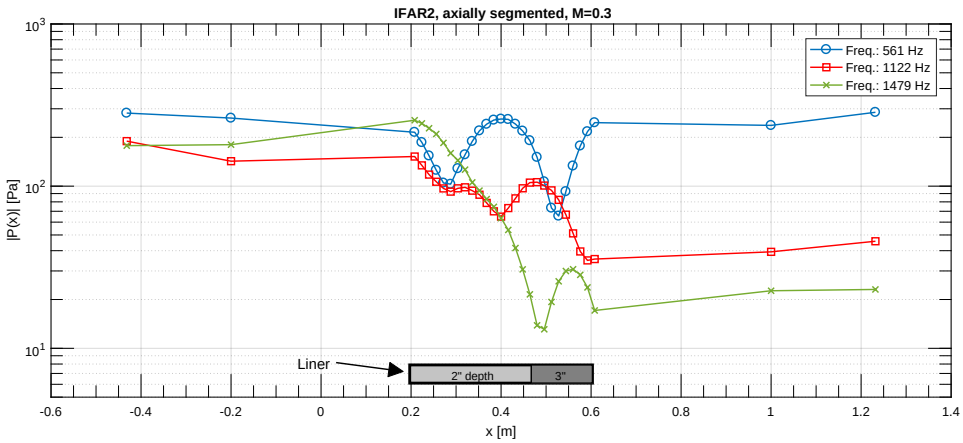

Figure 12. Axial pressure profiles with **IFAR2** liner sample at centerline Mach number 0.3 for three different frequencies: 561 Hz (blue line; low dissipation), 1122 Hz (red line; first dissipation maximum) and 1479 Hz (red line; second dissipation maximum).

The **IFAR2** liner with axial segmentation in Figure 12 provides two different frequencies with significant sound pressure reduction corresponding to the two dissipation peaks (see Figure 10). The first frequency of 1122 Hz (red line) shows a sound pressure reduction above the second liner segment (D3) at 0.467 m $< x < 0.603$ m. For the second frequency of 1479 Hz (green line), the sound pressure is mainly reduced in the liner segment with the lower cavity depth D2 comparable to the **IFAR1** sample with the same cavity depth. The pressure profile of a frequency with a low dissipation coefficient, here 561 Hz (blue line), is again mainly dominated by a standing wave pattern with little reduction in the sound pressure amplitude along the duct axis (x).

Wave number determination

The next step toward the impedance eduction is the determination of the axial wave numbers of all existing modes in the lined section. Here, a combination of two different methods (Kumaresan and Tufts (KT) method and Matrix Pencil (MP) method) combined with a manual sorting procedure was applied. The KT and MP methods are explained in detail in Weng et al.[6,13,14] and are only briefly introduced here.

The **KT method** is a Prony-like method. It detects the system poles of the acoustic wave field description by finding the roots of a linear prediction polynomial. The corresponding linear system of equations of the polynomial coefficients is solved in advance via a singular value decomposition (SVD). In order to select only the duct-mode-related singular values and to exclude noise-related contributions, the SVD is truncated by a criterion based on the minimum description length (MDL)[15].

While the KT method finds the system poles in two steps (solving the linear system of prediction equations and finding the roots of the prediction polynomial), the **MP method** finds the system poles and therewith the duct mode wave numbers directly by solving a generalized eigenvalue problem, called “matrix pencil”. The MP methods involves a certain prefiltering of the noise-contaminated data by performing also a truncated SVD (similar to the KT method). Here, again, the MDL approach is

used to estimate the relevant duct-mode-related singular values and reject or reduce noise influences. Compared to the KT method, the MP method is able to identify the modes propagating in both axial duct directions (downstream: x^+ and upstream: x^-) at the same time. Previous investigations on the performance of these two wave number determination methods[13] revealed that it may be beneficial to apply both methods together in practice since both methods behave different at low signal-to-noise ratios which allows a manual selection of the resulting wave numbers based on a plausibility assessment. The major plausibility criterion here is a continuous and smooth wave number function with respect to the frequency for each mode.

The careful determination of the dominating wave numbers becomes extremely important when a so called "mode crossing" appears in the lined section. "Mode crossing" denotes the change of the least attenuated mode from the fundamental mode ("plane wave") to a next higher order mode above a certain frequency. This higher order mode is then less damped than the fundamental mode. This effect was observed especially at liner samples with a low resistance value and earlier described for example in detail by Schulz et al.[16].

Here, this mode crossing also appears in the no flow and low Mach number flow cases for the **IFAR1** and **IFAR2** liner samples due to their fairly high facesheet porosity (about 12%) and the corresponding low wall resistance. Figure 13 shows the wave numbers for the **IFAR1** sample without grazing flow (upper plot: real part; lower plot: imaginary part) with an excitation from upstream (speaker A). Above a frequency of about 1300 Hz (dashed blue line), the absolute value of the imaginary part (describing the damping of the wave) of the fundamental mode (mode 0; black line) exceeds the corresponding value of the next higher order mode (mode 1; red line). This indicates that above this frequency the dominating, energy transporting duct mode changes to this higher order mode which should be accordingly selected for the impedance eduction procedure.

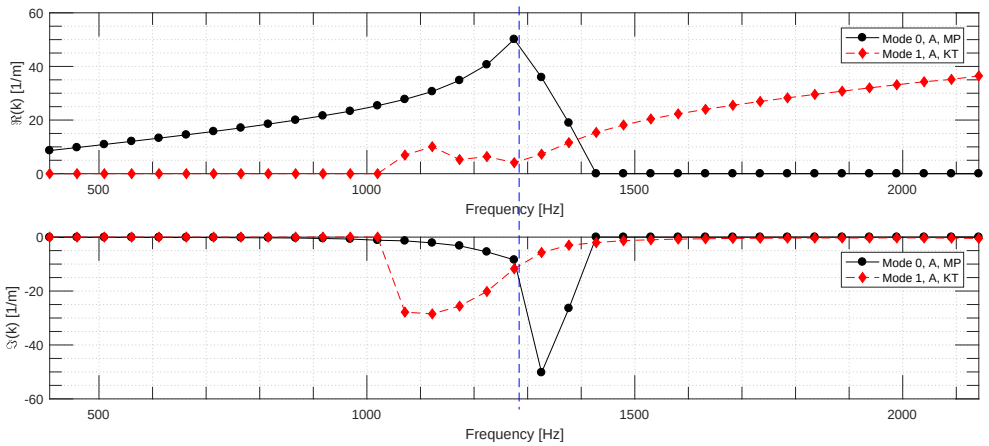

Figure 13. Real part (above) and imaginary part (below) of the determined wave numbers for **IFAR1** liner sample in the no grazing flow case with mode crossing between 1275 Hz and 1326 Hz (dashed blue line).

Impedance eduction from DLR measurements and comparison to NASA results

In general the test rig setup and the test procedure at the DUCT-R allows different techniques, modal based and nonmodal based, to educe the impedance. A comparative study of these methods was presented in earlier work.[6] In the framework of this IFAR liner benchmark the primary focus was set on the modal based techniques applying the determined wave numbers as described above.

Following the description of the acoustic pressure field for each mode by $\tilde{p} = \hat{p}(y)e^{-ikx}$, with the axial wave number of the respective mode k, the Convected Helmholtz Equation (CHE) reduces to a one-dimensional form:

$$\frac{\mathrm{d}^2\hat{p}}{\mathrm{d}y^2} + k_y^2\hat{p} = 0, \tag{15}$$

where $k_y^2 = k_0^2[(1 - M_{\mathrm{avg}}\Gamma)^2 - \Gamma^2]$ is the wall-normal wave number squared, $k_0 = \omega/c_0$ is the free-space wave number, ω is the angular frequency, c_0 is the reference speed of sound, $\Gamma = k_x/k_0$ is the dimensionless axial wave number and M_{avg} is the Mach number averaged over the duct cross section. With the Ingard-Myers condition[3,17] at $y = 0$ (liner surface) and the hard-wall boundary condition at $y = H$, the following nonlinear dispersion relation can be derived[18] from Equation 15:

$$\zeta = \frac{\mathrm{i}k_0\left(1 - M_{\mathrm{avg}}\Gamma\right)^2}{k_y \tan\left(k_y H\right)}. \tag{16}$$

Once the wave number Γ of a mode is determined following the procedure described in the previous section, the normalized liner impedance ζ can be calculated from Equation 16. Since the calculation is purely analytic and iteration-free, this eduction method is referred to as the straightforward method by Jing et al.[18] .

The impedance results obtained by DLR for the **IFAR1** liner sample are shown in Figure 14 (left: resistance $\Re(\zeta)$; right: reactance $\Im(\zeta)$). Without grazing flow (red squares) the resistance is fairly low (≈ 0.2) and nearly constant over the measured frequency range (400 Hz - 2100 Hz). The reactance shows a resonator typical curve progression from negative values to positive values crossing the zero at the resonance frequency of about 1500 Hz. Under low grazing flow conditions with a centerline Mach number of $M = 0.1$ (blue circles), the resistance slightly increases while the reactance does not change very much. With a grazing flow Mach number of $M = 0.3$ (black diamonds), the resistance increases as expected up to values between 0.5 and 0.7. Here, the reactance shows a shift of the resonance frequency to approximately 1600 Hz.

The corresponding values from the NASA GFIT test rig are also plotted in Figure 14 for the no flow case (green triangles) and for the case with a centerline Mach number of $M = 0.3$ (orange triangles). It should be noted that even with the same measured centerline Mach number the spatial Mach number distribution in the duct cross section is most likely somehow different between the GFIT test rig and the DUCT-R due to the different cross-sectional dimensions and the different axial duct length. However, the comparison of the resistance (Figure 14; left) and reactance (Figure 14; right) data show a very close match between DLR and NASA results. Only for lower frequencies below around 800 Hz some deviations (in the order of 30% for the reactance and the resistance with flow Mach number of 0.3) can be observed.

For the **IFAR2** liner samples, the wave number determination described in the previous section has been applied for each of the two axial sections of the liner sample (with different cavity depths) by

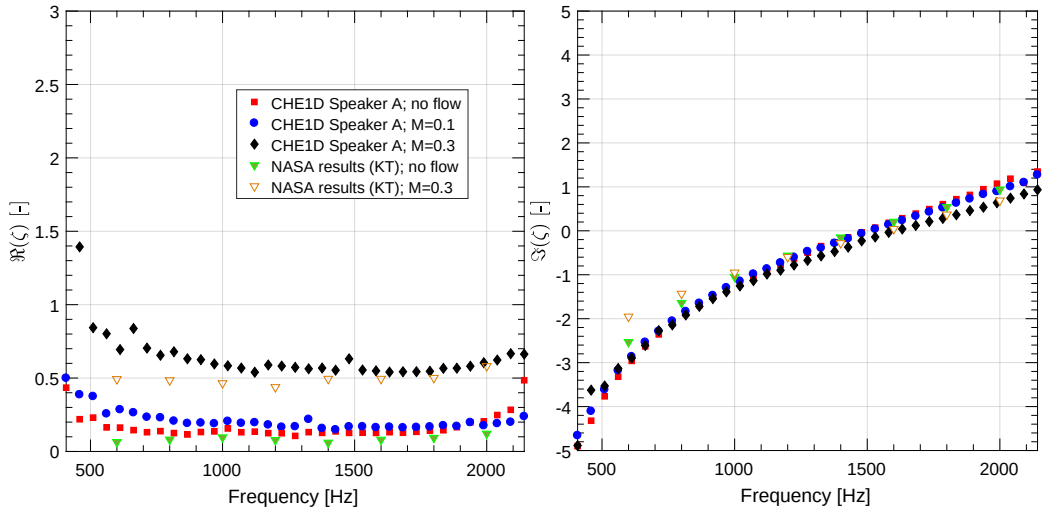

Figure 14. Real part (resistance; left) and imaginary part (reactance; right) of the educed liner impedance from DLR measurements for the **IFAR1** liner sample for three flow cases (no flow: filled red squares; $M = 0.1$: filled blue circles; $M = 0.3$: filled black diamonds). NASA results: no flow: filled green triangles; $M = 0.3$: open orange triangles.

selecting the appropriate face-to-face microphones in each section. The lower number of microphones used for the impedance evaluation of each section causes a higher scattering and uncertainty of the wave number values especially for the second liner segment where only 5 microphones for the no flow case and 8 microphones for the Mach 0.3 case could be employed. A sensitivity study (not shown here) revealed that relatively small errors in the wave number in the order of few percent can have a high impact on the uncertainty of the impedance results at certain frequencies. This is caused by the nonlinear relationship given by Equation 16, which magnifies measurement errors of the wave number at frequencies with a greater distance to the resonance frequency of the liner.

Figure 15 displays the impedance values for the first liner segment of **IFAR2** (**IFAR2-Pt.1**; D2) for two flow conditions. The corresponding NASA results are added in blue symbols. With respect to the resistance (Figure 15; left), the DLR values match very well the NASA data. The DLR data exhibit with grazing flow (black diamonds) only minor scattered resistance results for low frequencies below 700 Hz (similar to the NASA data). With grazing flow ($M = 0.3$), there is some systematic deviation in the reactance (Figure 15; right) between DLR (black diamonds) and NASA (blue diamonds) observable for low frequencies below 1100 Hz. This behaviour is not fully understood yet.

The impedance for the second part (**IFAR2-Pt.2**; D3) in Figure 16 indicates stronger scattered values for low frequencies $<$700 Hz and above $\approx$ 1500 Hz-1700 Hz especially for the grazing flow case for both the DLR (black stars) as well as the NASA (blue stars) data. This is presumably caused by the decreased signal-to-noise ratio with grazing flow. However, the reactance zero crossing and therewith the

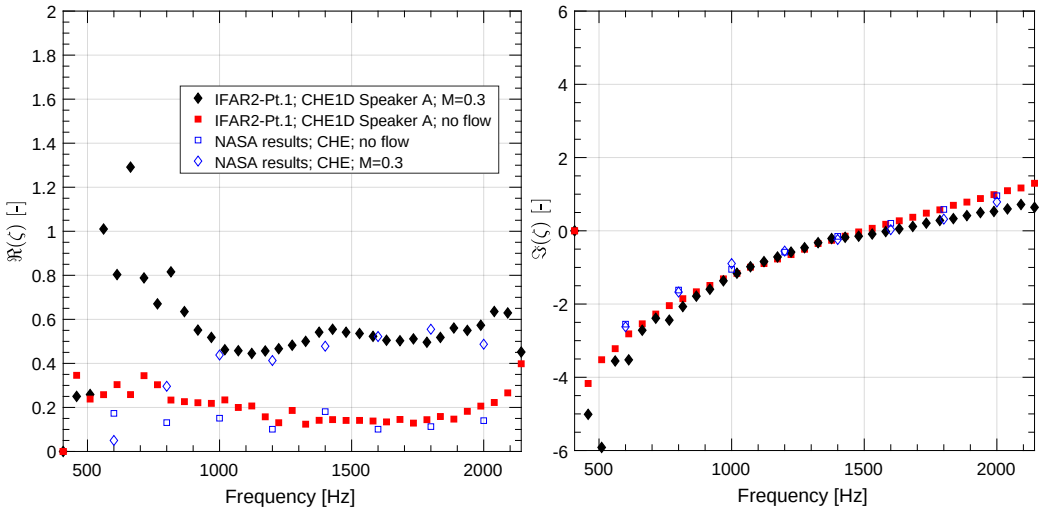

Figure 15. Real part (resistance; left) and imaginary part (reactance; right) of the educed liner impedance for the first part of the **IFAR2** liner sample (**IFAR2-Pt.1**; cavity depth D2) for two flow cases (no flow: filled red squares, $M = 0.3$: filled black diamonds) compared to the NASA results (no flow: open blue squares, $M = 0.3$: open blue diamonds).

liner resonance frequency is identified reasonably accurately to $\approx$ 1050 Hz for the **IFAR2-Pt.2** (D3; no flow) segment.

Comparing the results from the constant depth sample **IFAR1** (D2) to the **IFAR2-Pt.1** data (also D2) in Figure 17 shows a close match between **IFAR1** (filled symbols) and the **IFAR2-Pt.1** (open symbols). Only for the low frequency range below 800 Hz, the results for the **IFAR2-Pt.1** segment show more scattered impedance values. This is caused by the shorter length which reduces the number of face-to-face microphones and thereby increases the uncertainty of the wave number determination (KT/MP).

Conclusion

In the framework of the IFAR liner benchmark Challenge #1, the comparison of the DLR to the NASA results was presented. Starting with the DLR additive manufacturing and test rig integration of two different liner samples - one with constant cavity depth (**IFAR1**; D2) and one axially segmented with two different cavity depths (**IFAR2**; D2, D3) - the entire processing and acoustic characterization can now be compared to other partners' contributions within the framework of this benchmark.

The **IFAR1** liner sample shows a dissipation behaviour typical for resonator liners with a distinct maximum damping frequency around 1300 Hz. In contrast, the **IFAR2** sample reveals two dissipation maxima related to the quarter-wavelength resonance frequencies of each liner segment, respectively.

The corresponding axial pressure profiles confirm this observation and provide some insight into the total sound pressure level at each microphone position for the different configurations. One key processing step for the impedance eduction is the determination of the axial wave numbers of the

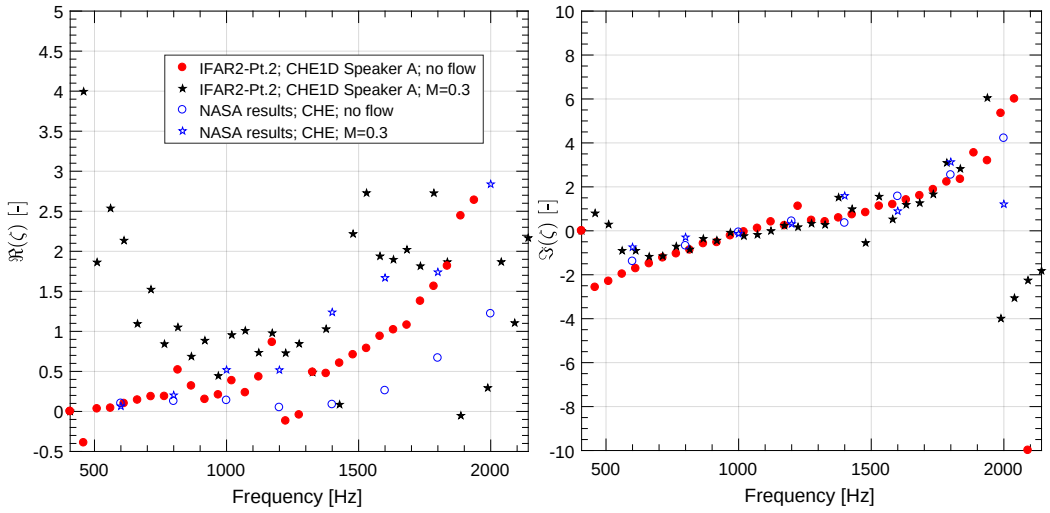

Figure 16. Real part (resistance; left) and imaginary part (reactance; right) of the educed liner impedance for the second part of the **IFAR2** liner sample (**IFAR2-Pt.2**; cavity depth D3) for two flow cases (no flow: filled red circles, $M = 0.3$: filled black stars) compared to the NASA results (no flow: open blue circles, $M = 0.3$: open blue stars).

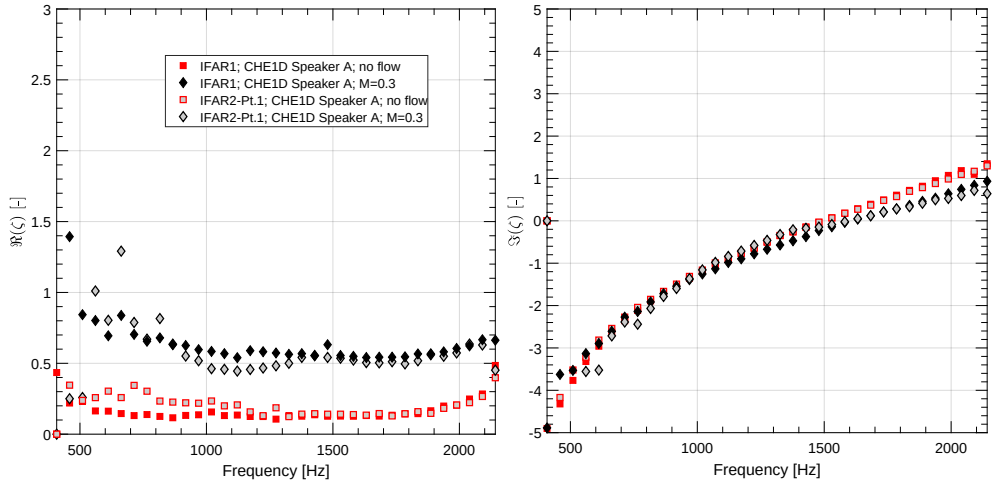

Figure 17. Real part (resistance; left) and imaginary part (reactance; right) of the educed liner impedance for the **IFAR1** liner sample (cavity depth D2) and the first part of the **IFAR2** liner sample (also cavity depth D2) for two flow cases. **IFAR1**: no flow: filled red squares, $M = 0.3$: filled black diamonds; **IFAR2** part 1: no flow: open red squares, $M = 0.3$: open black diamonds.

dominating modes in the lined sections. Hereby, a combination of two methods (KT/MP) with a specific truncation algorithm (MDL criterion) was applied to the data of the face-to-face microphones above the lined wall. A crucial processing component is here the manual mode selection based on a plausibility assessment.

Different, modal-based and nonmodal-based impedance eduction techniques are available at DLR. For the sake of brevity, only the results of the so-called straightforward method, based on an analytic solution of the one-dimensional Convected Helmholtz Equation (CHE1D), were presented. In this framework, also another modal-based impedance eduction method by solving the Pridmore-Brown equation over the full duct cross-section (PBE-CroSec method) was applied. Although PBE-CroSec takes into account visco-thermal losses as well as shear flow effects, in this case the method yields results fairly similar to the CHE1D.

Impedance eduction for the constant depth liner sample **IFAR1** shows reasonable results for the different grazing flow cases. The wave number determination for the two different axial parts of the segmented liner **IFAR2** appears to be more challenging. One main reason here is the reduced number of microphones (e.g., for the second part of **IFAR2** only 5-8 microphones compared to 19-20 microphones for **IFAR1**). The strong scattering behaviour within the impedance results can be explained by the strong nonlinear relation of the impedance and the axial wave number. Small uncertainties in the wave number values result in large variations of the educed impedance data. This applies especially for the shorter segment **IFAR2-Pt.2**. Due to a decreased signal-to-noise ratio, this effect is even further augmented under grazing flow conditions.

The comparison to the NASA impedance results shows a very good agreement for both liner samples. The overall evaluation demonstrates the liner impedance eduction capability even for complex nonhomogeneous liner samples.

Acknowledgements

The authors highly appreciate the support of Wolfram Hage and Sebastian Kruck in carefully manufacturing and post processing the liner samples.

References

1. Jones MG, Watson WR, Nark DM et al. Impedance eduction for multisegment liners. In *2018 AIAA/CEAS Aeroacoustics Conference, June 25-29, 2018, Atlanta, Georgia*. AIAA 2018-3441.
2. Jones MG, Nark DM and Howerton BM. Overview of liner activities in support of the international forum for aviation research. In *2019 AIAA/CEAS Aeroacoustics Conference, May 20-23, 2019, Delft, The Netherlands*. AIAA 2019-2599.
3. Myers MK. On the acoustic boundary condition in the presence of flow. *Journal of Sound and Vibration* 1980; 71(3): 429–434.
4. Busse-Gerstengarbe S, Bake F, Enghardt L et al. Comparative study of impedance eduction methods, Part 1: DLR tests and methodology. In *19th AIAA/CEAS Aeroacoustics Conference, 27-29 May 2013, Berlin, Germany*. AIAA-2013-2124.
5. Schulz A, Weng C, Bake F et al. Modeling of liner impedance with grazing shear flow using a new momentum transfer boundary condition. In *23rd AIAA/CEAS Aeroacoustics Conference, 5 - 9 June 2017, Denver, CO*. AIAA 2017-3377.

6. Weng C, Enghardt L and Bake F. Comparison of non-modal-based and modal-based impedance eduction techniques. In *24th AIAA/CEAS Aeroacoustics Conference, 25 - 29 June 2018, Atlanta, Georgia*.
7. Lahiri C, Sadig S, Gerendás M et al. Establishment of a high quality database for the acoustic modeling of perforated liners. *Journal of Engineering for Gas Turbines and Power* 2011; 133: 1–9.
8. Ronneberger D. *Genaue Messung der Schalldämpfung und der Phasengeschwindigkeit in durchströmten Rohren im Hinblick auf die Wechselwirkung zwischen Schall und Turbulenz*. Habilitation thesis, Universität Göttingen, 1975.
9. Brandes M. *Optimierung eines Meßvervahrens zur Bestimmung von akustischen Parametern im durchströmten Rohr*. Diploma thesis, Universität Göttingen, 1992.
10. Enghardt L. *Bestimmung akustischer Streufaktoren im durchströmten Rohr - Optimierung von Mikrofonanordung und Messprozedur*. Diploma thesis, Universität Göttingen, 1992.
11. Blokhintsev DI. Acoustics of a nonhomogeneous moving medium. Technical Memorandum 1399, NACA, 1956. Originally published 1946 in russian.
12. Morfey CL. Acoustic energy in non-uniform flows. *Journal of Sound and Vibration* 1971; 14(2): 159–170.
13. Weng C, Schulz A, Ronneberger D et al. Impedance eduction in the presence of turbulent shear flow using the linearized navier-stokes equations. In *23rd AIAA/CEAS Aeroacoustics Conference, 5 - 9 June 2017, Denver, CO*. AIAA 2017-3182.
14. Weng C, Schulz A, Ronneberger D et al. Flow and viscous effects on impedance eduction. *AIAA Journal* 2018; 56(3): 1118–1132. DOI:10.2514/1.J055838.
15. Wax M and Kailath T. Detection of signals by information theoretic criteria. *IEEE Transactions on Acoustics, Speech, and Signal Processing* 1985; 33(2): 387–392. DOI:10.1109/TASSP.1985.1164557.
16. Schulz A, Bake F, Enghardt L et al. Impedance eduction of acoustic liners based on four different levels of physical modeling. In *22th AIAA/CEAS Aeroacoustics Conference, 30 May-1 June 2016, Lyon, France*. AIAA 2016-2726.
17. Ingard U. Influence of fluid motion past a plane boundary on sound reflection, absorption, and transmission. *Journal of the Acoustical Society of America* 1959; 31: 1035–1036.
18. Jing X, Peng S and Sun X. A straightforward method for wall impedance eduction in a flow duct. *Journal of the Acoustic Society of America* 2008; 124(1): 227–234.